

Confinement-induced resonances in anharmonic waveguidesShi-Guo Peng,^{1,2} Hui Hu,² Xia-Ji Liu,² and Peter D. Drummond²¹*Department of Physics, Tsinghua University, Beijing 100084, China*²*Centre for Atom Optics and Ultrafast Spectroscopy, Swinburne University of Technology, Melbourne 3122, Australia*

(Received 29 June 2011; published 12 October 2011)

We develop the theory of anharmonic confinement-induced resonances (ACIRs). These are caused by anharmonic excitation of the transverse motion of the center of mass (c.m.) of two bound atoms in a waveguide. As the transverse confinement becomes anisotropic, we find that the c.m. resonant solutions split for a quasi-one-dimensional (1D) system, in agreement with recent experiments. This is not found in harmonic confinement theories. A new resonance appears for repulsive couplings ($a_{3D} > 0$) for a quasi-two-dimensional (2D) system, which is also not seen with harmonic confinement. After inclusion of anharmonic energy corrections within perturbation theory, we find that these ACIRs agree extremely well with anomalous 1D and 2D confinement-induced resonance positions observed in recent experiments. Multiple even- and odd-order transverse ACIRs are identified in experimental data, including up to $N = 4$ transverse c.m. quantum numbers.

DOI: [10.1103/PhysRevA.84.043619](https://doi.org/10.1103/PhysRevA.84.043619)

PACS number(s): 03.75.Hh, 03.75.Ss, 05.30.Fk

I. INTRODUCTION

Ultracold low-dimensional atomic gases show unique quantum properties and have attracted a great deal of interest. For a one-dimensional (1D) Bose gas [1–3], the finite-temperature correlations predicted for a Tonks-Girardeau gas [4,5] have been experimentally verified [6,7], and a crossover to a nonequilibrium super-Tonks-Girardeau gas has been realized [8]. For a two-dimensional (2D) geometry, the Berezinskii-Kosterlitz-Thouless phase transition was predicted [9,10] and subsequently observed in experiment [11]. In these experiments, one or two spatial degrees of freedom are removed by introducing tight confinement via an optical lattice or a tightly focused anisotropic dipole trap.

Atomic interactions can also be tuned precisely by means of a molecular Feshbach resonance in an external magnetic field [12–14]. This allows an effective contact interaction with scattering length a_{3D} to be created, with scattering lengths that can be varied over a wide range of positive and negative values. Owing to these methods, low-dimensional atomic gases now provide a high degree of control for tests of fundamental many-body physics in reduced dimensions. These systems are often much simpler than condensed-matter physics experiments, which have complex crystal structure, interactions, and disorder.

Confinement-induced resonance (CIR) is one of the most intriguing phenomena found in low-dimensional systems. These were first predicted theoretically by Olshanii [15], who considered a two-body s -wave scattering problem in a quasi-1D trap with cylindrically symmetric transverse harmonic confinement. The CIR can be understood as a novel type of Feshbach resonance, where the transverse ground mode and the manifold of molecular internally excited modes play the roles of the open and closed channels, respectively [16]. Related effects occur in mixed dimensional traps [17,18]. A direct generalization of Olshanii's theory to anisotropic transverse confinement shows that there is only one harmonic CIR (HCIR), no matter how large the transverse anisotropy [19]. For large anisotropy, this theory crosses over smoothly to the case of a quasi-2D trap, where a single HCIR occurs with a negative s -wave scattering length, $a_{3D} < 0$ [20–22].

There have been a number of related experimental investigations, which in some cases appear to contradict each other. In the recent Innsbruck Cs experiment with a quasi-1D geometry [23], two or more resonances were observed as the transverse confinement became more and more anisotropic. For a quasi-2D geometry, some experiments have observed 2D resonances on the attractive side with $a_{3D} < 0$ [24], while others have resonances on the repulsive side with $a_{3D} > 0$ [23,25]. The observations of both multiple resonances and 2D resonances with repulsive interactions are in disagreement with standard HCIR predictions [20–22].

In this paper, a detailed explanation is proposed for these anomalous resonances. The mechanism is that the new resonances are due to center-of-mass (c.m.) excitations of molecules or atom pairs. These have a different character than the excitation of internal molecular degrees of freedom found in the Olshanii approach and its generalizations. The new c.m. resonances can only become coupled to the input state by anharmonic terms in the trapping potential. Hence, we term these effects anharmonic confinement-induced resonances (ACIRs). The ACIRs cannot occur in harmonic traps due to Kohn's theorem [26]. However, they are certainly observable in current ultracold atomic physics experiments, which have relatively large anharmonicities.

The coupling of the c.m. motion to the relative motion gives additional degrees of freedom not found with parabolic traps. This causes a series of additional scattering resonances due to the mixing of c.m. and relative motion. The nonlinear mixing caused by anharmonic terms in the potential makes these phenomena analogous to frequency-mixing effects found in nonlinear optics. They provide a fundamentally new pairing mechanism, which may lead to new opportunities for quantum engineering in atomic, photonic, or acoustic waveguides. Our results are therefore qualitatively different than harmonic CIR. We predict both multiple 1D resonances and 2D resonances with repulsive interactions. Both results are in quantitative agreement with experiment.

We note that this possibility was also envisaged in three earlier papers. Peano *et al.* [27] addressed the general idea, although using a different technique and for a different type of trap. Kestner and Duan [28] treat anharmonic resonance

in a double well. In a more recent investigation, parallel to our own, Sala *et al.* [29] have also concluded that the recent Innsbruck experiments provide evidence for ACIRs. The main differences in the treatment are that we have accurately calculated the size of the anharmonic resonance shifts, as well as giving quantitative estimates of relevant parameters. We also compare our theory with the observed multiple resonances, including even- and odd-order c.m. resonances.

The paper is arranged as follows. We first analyze the types of transverse excitations available and the operational processes that can lead to the observed resonances (Sec. II). In Sec. III, a Hamiltonian model of nonlinear CIR is presented, by introducing anharmonic perturbations in the Hamiltonian. In Sec. IV, this is analyzed using perturbation theory for the 1D case. The results are compared to experiments on anisotropic traps, showing the observed splitting is well explained with the anharmonic c.m. resonance ACIR model. Next, we consider results for the case of large trap anisotropies and demonstrate that the observed resonances can be quantitatively explained with excellent accuracy by considering multiple resonances with both even- and odd-order c.m. transverse quantum numbers. A similar calculation is carried out for a quasi-2D system in Sec. V, which is also compared with experiment. The main results are summarized in Sec. VI.

II. TWO-BODY CIR PHYSICS

In recent one- and two-dimensional confinement-induced resonance experiments, there are many observed resonances not explained by conventional CIR theory. In two dimensions, resonances are observed for $a_{3D} > 0$ [the Bose-Einstein condensate side of the resonance], which is the opposite to that expected in the usual theory. Similarly, unexplained multiple resonances occur for one-dimensional CIRs with anisotropic transverse confinement. These are also not predicted by the simple two-particle model [15] with linear confinement. However, the experiments have some features not included in this idealized model, and the obvious question is: Which experimental properties are responsible for the additional observed resonances?

A. Harmonic CIR solutions

The possible modes of excitation of a pair of atoms in a transverse potential are illustrated in Fig. 1. The c.m. mode is shown in Fig. 1(a), with two atoms moving together. This is not coupled to the atomic ground state in a harmonic trap, due to Kohn's theorem. The relative motion mode is shown in Fig. 1(b), with an excitation of the relative coordinate. This is the usual harmonic confinement-induced resonance in a one-dimensional waveguide with a transverse parabolic potential. The HCIR is simply the first *internally* excited resonance of the two-body ground state.

However, there is a subtlety here. Both types of excitation are adiabatic continuations of the transversely excited free-particle states, as the interparticle interaction is increased. The free-particle states have both c.m. quantum numbers N_x, N_y , and internal quantum numbers, n_x, n_y . Therefore, there are a large number of possible excited states that could, in principle,

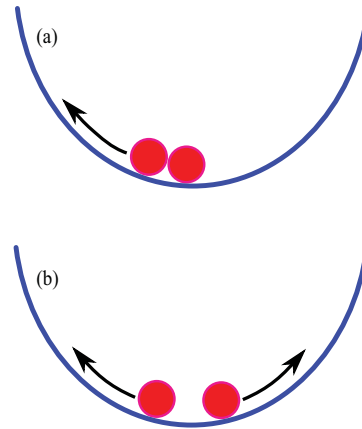


FIG. 1. (Color online) (a) Illustration of an ACIR, in which two atoms are driven in a moleculelike excited state with a transverse c.m. motion in the trap. Both atoms move together, to give a transverse resonance of the c.m. degree of freedom. This is only coupled to the atomic ground state if the potential is anharmonic. (b) Illustration of an HCIR, in which the atoms move in relative motion to give an excited state rather like a conventional vibrational excited state of a molecule.

be coupled to the atomic ground state in a Feshbach type of resonance.

In a rotationally symmetric model, both the internal and c.m. excited states near $2\hbar\omega$ are degenerate in energy and cannot lead to distinct resonances even if coupled to the incoming states. If there is no rotational symmetry, this degeneracy is broken, leading to the possibility of multiple resonances. Experimentally there is more than one resonance in the recent Innsbruck experiment [23]. Owing to the similarity with the HCIR predictions [15], these were initially identified as conventional harmonic CIRs, corresponding to excitations of internal degrees of freedom.

However, an analysis of the anisotropic case [19] indicates that internally excited two-body states only give rise to only a *single* CIR. We note that Kohn's theorem [26] prohibits the excitation of c.m. resonances from incoming states with no transverse momentum, if the confinement is parabolic. One may ask why there are not multiple CIR eigenstates with different internal energies due to the different confinement strength in orthogonal trap directions. The reason for this is due to the singular nature of the interaction.

Consider what happens to a single particle in a rotationally symmetric potential, which corresponds to the internal quantum numbers in a relative coordinate picture of a two-particle problem. In a 2D system of noninteracting particles in a harmonic oscillator potential, the ground state has $n_x = n_y = 0$. The internally excited states can therefore be labeled either by their internal harmonic oscillator quantum numbers for relative motion or by their angular momentum quantum numbers. For this, one can have $n_x = n_y = 1$, or else a radial quantum number n_r and a magnetic quantum number m . Owing to the singular potential at the origin, only *s*-wave incoming states with $m = 0$ experience any coupling. This leads to a relatively low-lying excited state due to the coupling and, hence, to a single CIR. This state is adiabatically deformed when the symmetry is broken, without leading to a second CIR.

This single degenerate CIR exists on the positive side of the Feshbach resonance, i.e., $a_{3D} > 0$, for a quasi-1D system. It transfers to the negative side, i.e., $a_{3D} < 0$, for a large asymmetry or a quasi-2D system. This last conclusion is compatible with other calculations of 2D CIR. However, these conclusions only take into account the *internal* energy of a two-particle state, not the c.m. energy.

B. Anomalous CIR experiments

In recent bosonic experiments on ultracold ^{137}Cs at Innsbruck [23], a strong, transversely anisotropic quasi-1D confinement is used to create an initially strongly repulsive ($a_{3D} > 0$) Tonks gas. This is followed by a sudden change in B field to a new value, resulting in a molecular loss signature for a resonance which is confinement dependent. Numerous multiple confinement-induced resonances are observed. There is even an unexpected resonance for $a_{3D} > 0$ in the 2D limit, which has also been measured using release energy data in fermionic ^6Li experiments [25]. All these observations contradict the harmonic waveguide theory given above.

However, it is important to recognize that the waveguide potentials in these experiments are generally anharmonic, so Kohn's theorem does not apply. Hence, there are more degrees of freedom available for excitation, since the c.m. quantum numbers must now be included in the description.

The interesting issue is whether these observed CIR effects can be explained as anharmonic resonances (ACIRs) due to center-of-mass excitations of resonant bound states [27–29]. This is illustrated by the two atoms moving together in Fig. 1(a). Such effects can only occur in an anharmonic trapping environment, which allows coupling between incoming scattering states with zero transverse excitation and an outgoing transverse c.m. excitation.

In another 2D experiment on ultracold ^{40}K at Cambridge [24], a CIR occurs on the attractive side of a Feshbach resonance, as expected. This experiment has a much lower anharmonicity than the Innsbruck experiment. It also uses a different technique to identify the resonance, employing rf spectroscopy rather than molecular losses. Thus, there are distinct resonance signatures used in the two published experiments. The Cambridge data appear to show evidence for anomalous resonance features on the $a_{3D} > 0$ side of the Feshbach resonance, but this effect is greatly reduced compared to the Innsbruck observations.

All Feshbach bound states have a bound molecular fraction [30] in which the atoms have a small separation. We conjecture that this molecular fraction is larger for (a) c.m. ACIRs, where the atoms are in a relative ground state, compared to (b) internally excited HCIRs, where the atoms are in a relative excited state. This would mean that c.m. excitations would have a relatively larger three-body recombination loss due to molecule formation. This is precisely the signature of the resonances used in the Innsbruck experiments. On the other hand, rf spectroscopy, used in the Cambridge experiments, has different characteristics. Thus, it is not unreasonable to expect the two experiments to have a different relative sensitivity to internal and c.m. molecular resonances.

III. ANHARMONIC WAVEGUIDES

For technical reasons explained below, current CIR experiments typically involve an anharmonic confinement mechanism. In such cases, the excitation of a c.m. degree of freedom can be coupled to input states with no transverse c.m. excitation. This coupling mechanism would explain observed anomalies, such as multiple resonances, that are different than those predicted using the standard parabolic confinement theory.

There are three possibilities which might allow resonant coupling to additional confinement-induced bound states through nonlinear mechanisms:

(1) The Kohn theorem only applies for parabolic confinement. Experimentally the optical confinement is sinusoidal and/or Gaussian, not parabolic. This allows direct coupling to $N_x = 2$ states, or even $N_x = 1$ states, depending on the type of anharmonicity.

(2) In some experiments the width of the Feshbach resonance is comparable to the separation of the transverse modes, allowing contributions from the molecular bound-state channel as well as the atomic channel. This still requires anharmonic coupling to access bound states having c.m. transverse energy.

(3) At high density the mean-field background potentials of the other atoms may provide an anharmonic effective potential which is not parabolic. In such cases, one may expect the collective oscillation frequencies to play a role.

Coupling to c.m. excitations is possible whenever the transverse response is nonlinear and the potential departs from a parabolic shape. This is not inconsistent with the ultracold atomic physics experiments, which generally involve sinusoidal laser trapping potentials. These are only approximately parabolic in the strongly confined limit. It is this possibility of nonlinear CIR due to anharmonic confinement which is explained below. Although related theoretical work that has been carried out includes one or the other of these effects, it is important to include *both* anisotropy and anharmonicity to fully explain the observed ACIRs.

A. Hamiltonian

In this paper, we consider the simplest model of nonlinear CIR, with a single-channel s -wave interatomic potential and an anharmonic trapping potential. We do not take into account either many-body corrections or explicit molecule formation channels [30]. This model is therefore applicable to relatively dilute quantum gases with a broad Feshbach resonance. To model the nonlinear CIR effect in greater detail, consider two atoms with mass m which are anisotropically confined in the transverse direction and can almost freely move in the z direction. Such a model can treat both a quasi-1D and quasi-2D experiments, by taking one of the trapping frequencies to zero. The Hamiltonian of the two atoms in a quasi-1D system is, therefore,

$$H = H_1 + H_2 + U(\mathbf{r}_1 - \mathbf{r}_2), \quad (3.1)$$

where

$$U(\mathbf{r}) = g_{3D} \delta(\mathbf{r}) \frac{\partial}{\partial r} r \quad (3.2)$$

is the atomic interaction for s -wave scattering described by a zero-range pseudopotential with interaction strength $g_{3D} = 4\pi\hbar^2 a_{3D}/m$ corresponding to a scattering length of a_{3D} , and H_i is a single-particle Hamiltonian including external potential and kinetic energy terms.

1. Anharmonic confinement potential

For dipole trapping experiments with 1D and 2D optical lattices, the trapping potential near a potential minimum at $\mathbf{r} = 0$ is due to an optical standing wave of the form

$$\begin{aligned} U^{\text{ext}}(\mathbf{r}) &= V_x(\mathbf{r}) \sin^2\left(\frac{2\pi x}{\lambda_x}\right) + V_y(\mathbf{r}) \sin^2\left(\frac{2\pi y}{\lambda_y}\right) \\ &\approx \frac{1}{2}m \left[\omega_x^2 x^2 \left(1 + \frac{\alpha_x x^2}{d_x^2} + \frac{\mathbf{r} \cdot \nabla V_x}{V_x^0} + \dots\right) \right. \\ &\quad \left. + \omega_y^2 y^2 \left(1 + \frac{\alpha_y y^2}{d_y^2} + \frac{\mathbf{r} \cdot \nabla V_y}{V_y^0} + \dots\right) \right]. \end{aligned} \quad (3.3)$$

Here, $V_{x,y}(\mathbf{r})$ are the two orthogonal slowly varying potential energy envelopes of standing waves due to the atomic dipole interactions with the two trapping lasers at optical wavelengths λ_x, λ_y . Thus, $V_{x,y}^0$ are potential well depths, leading to trap frequencies ω_x, ω_y in the x, y directions. We have used a scale length of the reduced oscillator lengths $d_{x,y} = \sqrt{2\hbar/m\omega_{x,y}}$ in each direction. It is also common to use the single-atom oscillator length definition of $a_{x,y} = \sqrt{\hbar/m\omega_{x,y}}$, which we use in comparisons with experiment in later sections.

To next order beyond the linear confinement approximation, we have introduced $\alpha_x, \alpha_y \ll 1$ as the dominant anharmonic parameters, so that

$$\begin{aligned} \omega_{x,y} &= \frac{2\pi}{\lambda} \sqrt{\frac{2|V_{x,y}^0|}{m}}, \\ \alpha_{x,y} &= \frac{-8\pi^2\hbar}{3\lambda^2 m \omega_{x,y}}. \end{aligned} \quad (3.4)$$

For plane waves, these quartic anharmonic terms are the lowest order possible. More generally, the potential may be neither parabolic nor sinusoidal. Examples of this include the potential found in an optical fiber, which can be engineered to any desired shape, and potentials found in experiments using magnetic trapping or focused Gaussian beams. For this reason, we expect cubic, quartic, and higher-order anharmonic parameters in any real experiment. However, the quartic term given above is due to spatial modulation on optical wavelength scales. This is generally larger than cubic anharmonic terms like $\mathbf{r} \cdot \nabla V_x$ caused by focusing effects.

For simplicity, we suppose that the dominant anharmonic effects are caused by anharmonic parameters $\alpha_{x,y}$, and the single-particle Hamiltonian is

$$\begin{aligned} H_i &= -\frac{\hbar^2}{2m} \nabla_{\mathbf{r}_i}^2 + \frac{1}{2} m \omega_x^2 x_i^2 \left(1 + \alpha_x x_i^2/d_x^2\right) \\ &\quad + \frac{1}{2} m \omega_y^2 y_i^2 \left(1 + \alpha_y y_i^2/d_y^2\right) \quad (i = 1, 2). \end{aligned} \quad (3.5)$$

TABLE I. Typical anharmonic parameters for CIR experiments using optical lattices, following data from Haller *et al.* (Cs) [23] and Fröhlich *et al.* (K) [24]. Quantitative values depend on the trap frequency, which is varied over a range of values.

Experiment	^{133}Cs	^{40}K
Trap frequency, ω	$2\pi \times 14.5$ kHz	$2\pi \times 80$ kHz
Wavelength, λ	1.064×10^{-6} m	1.064×10^{-6} m
Atomic mass, m	2.22×10^{-25} kg	0.6635×10^{-25} kg
Length, $d_{x,y}$	0.102×10^{-6} m	0.08×10^{-6} m
Anharmonicity, $\alpha_{x,y}$	-0.121	-0.075

Thus, the trapping Hamiltonian (3.1) has the form of a harmonic Hamiltonian H_h plus anharmonic terms H_a^x and H_a^y in the x and y directions, respectively:

$$H_1 + H_2 = H_h + H_a^x + H_a^y = H_h + H_a. \quad (3.6)$$

Next, we can estimate typical parameter values in recent experiments, as shown in Table I. We note that in the Innsbruck experiments with relatively large observed anomalies, the dimensionless anharmonic parameter was typically 12%, which is substantially larger than in the case of the Cambridge experiment, with an anharmonicity of 7.5%. These parameters are calculated for alkali-metal atoms, micron-wavelength lasers, and typical 10–100-kHz trap frequencies. Obviously, large changes in anharmonicities are easily obtained by changing any of the relevant factors.

These anharmonic parameters lead to energy shifts in the ACIRs, which we calculate below. More importantly, any type of anharmonic potential allows a coupling between relative and c.m. motion, which is otherwise prohibited due to the Kohn theorem.

B. Center-of-mass energies

We can now make a preliminary estimate of atomic and molecular energies in the two-particle sector, given the anharmonic trapping potential. These estimates assume sufficiently tight internal binding so that only the c.m. energies are changed by the anharmonicity. While this is not accurate near threshold, it allows an estimate of the size of anharmonic perturbation energies. It is also used to check the validity of subsequent results in the tight-binding limit.

1. Atomic energy

For a single particle, the perturbation theory solution including the anharmonic parameter is well known. We can calculate how the free atomic energy,

$$E_A^{(0)} = (n_x + \frac{1}{2})\hbar\omega_x + (n_y + \frac{1}{2})\hbar\omega_y, \quad (3.7)$$

is changed by the anharmonic perturbation. To first order in perturbation theory, the modified transverse ground-state energy is an elementary perturbation theory result, such that

$E_A = E_A^{(0)} + E_A^{(1)}$, where

$$\begin{aligned} E_A^{(1)} &= \langle \psi_{n_x, n_y} | H_a | \psi_{n_x, n_y} \rangle \\ &= \frac{3}{16} [2n_x(n_x + 1) + 1] \hbar \omega_x \alpha_x + x \leftrightarrow y. \end{aligned} \quad (3.8)$$

Here, $|\psi_{n_x, n_y}\rangle$ is the single-particle eigenstate of H_h , which is treated as the zero-order wave function. For a threshold resonance experiment, the incoming total energy of two atoms initially in a transverse and longitudinal ground state is therefore

$$E_{\text{scatt}} = \hbar \omega_x (1 + \frac{3}{8} \alpha_x) + (x \leftrightarrow y). \quad (3.9)$$

Using the numbers in Table I, this indicates that the scale of anharmonic energy perturbations should be around 5–10% of the transverse trap frequency for the parameters of recent experiments.

2. Molecular energy

In the c.m. relative-coordinate frame, with $\mathbf{R} = (\mathbf{r}_1 + \mathbf{r}_2)/2$, $\mathbf{r} = \mathbf{r}_1 - \mathbf{r}_2$, the harmonic term is

$$\begin{aligned} H_h &= H_h^{\text{c.m.}} + H_h^{\text{rel}} \\ &= -\frac{\hbar^2}{2M} \nabla_{\mathbf{R}}^2 + \frac{1}{2} M (\omega_x^2 X^2 + \omega_y^2 Y^2) - \frac{\hbar^2}{2\mu} \nabla_{\mathbf{r}}^2 \\ &\quad + \frac{1}{2} \mu (\omega_x^2 x^2 + \omega_y^2 y^2) + U(\mathbf{r}), \end{aligned} \quad (3.10)$$

and the anharmonic term is

$$\begin{aligned} H_a &= H_a^x + H_a^y \\ &= \frac{\alpha_x m \omega_x^2}{2d_x^2} \left(2X^4 + 3X^2x^2 + \frac{x^4}{8} \right) + x \leftrightarrow y. \end{aligned} \quad (3.11)$$

Here, $\mathbf{r} = (x, y, z)$, $\mathbf{R} = (X, Y, Z)$, and $M = 2m$, $\mu = m/2$ are the mass of the c.m. and the reduced mass, respectively.

As a point of reference for the more detailed calculations given below, we now consider how the c.m. energy of molecular bound states changes due to anharmonicity. For a broad Feshbach resonance, with strong binding so that the internal molecular energy is not changed by the waveguide, the internal molecular bound-state energy in free space for an attractive interaction is known to be

$$E_b^{3D} = -\frac{\hbar^2}{m a_{3D}^2}. \quad (3.12)$$

For a tightly bound molecule described only by the c.m. coordinates (X, Y) , the oscillator frequencies are ω_x, ω_y as before. To first order in perturbation theory, the additional c.m. energy $E_{\text{c.m.}}$ of a tightly bound molecular state is therefore

$$E_{\text{c.m.}} = E_{\text{c.m.}}^{(0)} + E_{\text{c.m.}}^{(1)}, \quad (3.13)$$

where $E_{\text{c.m.}}^{(0)} = (N_x + \frac{1}{2})\hbar\omega_x + (N_y + \frac{1}{2})\hbar\omega_y$, and

$$\begin{aligned} E_{\text{c.m.}}^{(1)} &= \langle \Psi_{N_x N_y} | H_a | \Psi_{N_x N_y} \rangle \\ &= \frac{3\hbar\omega_x\alpha_x}{32} [1 + 2N_x(N_x + 1)] + x \leftrightarrow y. \end{aligned} \quad (3.14)$$

Here, $|\Psi_{N_x, N_y}\rangle$ is the single-molecule eigenstate of H_h , again treated as the zero-order wave function, and $E_{\text{c.m.}}^{(0)}$ and $E_{\text{c.m.}}^{(1)}$ are the harmonic and anharmonic contributions, respectively, to

the c.m. molecular energy. The reduced anharmonic correction compared to the free atomic case is due to the reduced spatial width of the wave function, caused by the increased molecular mass compared to an atom.

C. Tightly bound resonance threshold

This allows us to make a relatively simple calculation. A threshold condition in the tight-binding limit is obtained from equating the total ground-state transverse energy of two atoms with the total molecular energy in a c.m. excited transverse state. It is convenient for later calculations to define a dimensionless bound-state energy relative to unbound atoms in a transverse waveguide as

$$\epsilon \equiv \frac{E_b}{\hbar\omega_y} - \frac{1}{2}(1 + \eta), \quad (3.15)$$

where $\eta = \omega_x/\omega_y$ is the anisotropy of the two transverse binding frequencies, and $E_b = E_b^{3D}$ in the strong-binding limit of interest here. The correction term of $-\frac{1}{2}(1 + \eta)$ is required to take account of the difference in the transverse confinement energies between the atoms and the molecular state, which does not occur in free space.

After including the anharmonic corrections and excitation energies from Eqs. (3.8) and (3.14), one obtains a resonance condition for *deeply* bound molecular ACIRs in an intuitive form as

$$E_{\text{scatt}} = E_b + E_{\text{c.m.}} \quad (3.16)$$

On transforming this to dimensionless form, we obtain

$$\begin{aligned} \epsilon + N_y + \alpha_y \left[\frac{3}{16} N_y(N_y + 1) - \frac{9}{32} \right] \\ + \eta \left\{ N_x + \alpha_x \left[\frac{3}{16} N_x(N_x + 1) - \frac{9}{32} \right] \right\} = 0. \end{aligned} \quad (3.17)$$

Clearly there are multiple resonances as N_x and N_y are varied, thus altering the c.m. quantum numbers of the excited transverse molecular states. The position of these resonances is largely determined by the quantum numbers, together with anharmonic shifts. In the next section, we show that wavefunction symmetries mean that the even-order resonances are directly coupled by the strong quartic anharmonicities α_x, α_y . Odd-order resonances are coupled through the relatively weaker cubic anharmonic terms due to the $\mathbf{r} \cdot \nabla V_x$ terms, which are physically caused by the slow variations in the Gaussian envelope function of the trapping lasers in these experiments.

The consequences are seen in Fig. 2, which shows the first two strongly coupled even-order c.m. resonances, as compared with the internally excited resonance position. The traditional HCIR state in a one-dimensional harmonic waveguide is identified by the solid line in Fig. 2. This curve is simply the first *internally* excited state of the two-body ground state [15,19]. One expects a CIR to occur whenever the solid curve crosses the lowest horizontal line, thus permitting a resonance to occur with incoming atoms near zero energy.

However, we see that there are also two further possibilities, spaced both above and below the internally excited resonance. These are the lowest-lying even-order ACIRs, which we expect to be the dominant excitations in the case of anharmonic waveguides. While this calculation is approximately correct

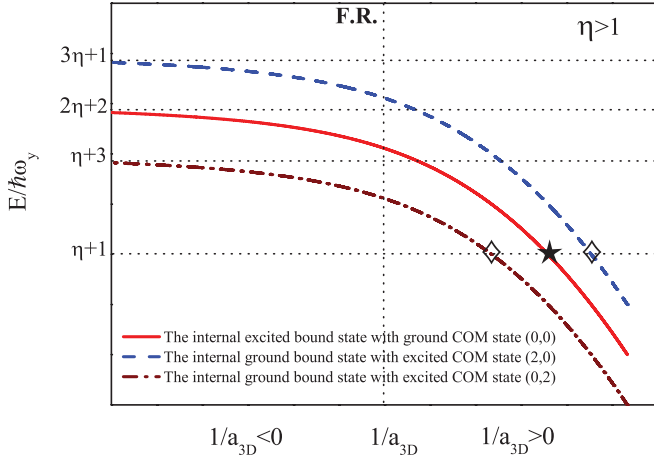


FIG. 2. (Color online) Diagram of the confinement-induced energy levels in an anisotropic trap or waveguide, with anisotropy η . The solid line is an internally excited two-particle ground state. The dashed lines correspond to c.m. excitations of the two-particle ground state. Confinement-induced resonance thresholds occur when these excited molecular states become resonant with two incoming free particles with zero momentum. This is indicated by a star in the internally excited CIR case, which is the only level coupled in the case of a harmonic trap. For anharmonic traps, these additional levels become coupled to input atomic states with zero transverse excitation and acquire additional anharmonic energy shifts.

and gives an excellent intuitive picture, we carry out a quantitative calculation in the following sections with the inclusion of the internal degrees of freedom as well.

IV. ANHARMONIC CIR IN A QUASI-1D WAVEGUIDE

While Eq. (3.17) is valid for a relatively deeply bound molecule, it neglects both anharmonic and waveguide corrections to the *internal* molecular energy E_b . The question of which transverse molecular quantum numbers N_x, N_y are accessible in terms of selection rules also needs to be addressed more carefully. In this section, we therefore treat the general case of a quasi-1D confining waveguide with an asymmetric confining potential. This case can be continuously changed to the limit of the 2D trap, which is treated in more detail in the following section. Owing to the small anharmonic parameter α , the anharmonic term H_a is treated as a perturbation to H_h .

A. Harmonic CIR

First, we consider the anisotropic waveguide *without* the anharmonic perturbation H_a . While this has been treated previously [19], we revisit it here as a first step to solving the anharmonic case. The origin of the confinement-induced resonance is due to two scattering atoms forming a virtual molecule via their *s*-wave interaction. The energy of the resulting two-atom quasibound state in a waveguide is written as

$$\begin{aligned} E_M^{(0)} &= E_{\text{c.m.}} + E_b \\ &= (N_x + \frac{1}{2})\hbar\omega_x + (N_y + \frac{1}{2})\hbar\omega_y + E_b. \end{aligned} \quad (4.1)$$

Here $E_{\text{c.m.}}$ is the energy of the c.m. excitation, (N_x, N_y) are the quantum numbers of the c.m., and E_b is the binding energy

of the two atoms. This becomes resonant with two incoming atoms near zero momentum when $E_M^{(0)} = E_{\text{scatt}}$, where E_{scatt} is the incoming free-particle energy. This is trivially given in the zero-momentum, harmonic case by

$$E_{\text{scatt}} = 2E_A^{(0)} = \hbar\omega_x + \hbar\omega_y. \quad (4.2)$$

By solving the eigenproblem of the relative Hamiltonian of the two atoms, H_h^{rel} , we can obtain the relation between the binding energy E_b and the 3D *s*-wave scattering length a_{3D} . This is known from previous work [19] by solving for the dimensionless energy ϵ of the molecular ground state, where $\epsilon \equiv E_b/\hbar\omega_y - (\eta + 1)/2$, as given in Eq. (3.15). We note that, just as with Eq. (3.15) in the previous section, the dimensionless energy ϵ is defined so that it includes the change in transverse confinement energies. With this definition, E_b reduces to the free-space binding energy in the limit of weak confinement or strong binding.

The dimensionless ground-state molecular energy ϵ is given by an implicit equation [19]:

$$\frac{d_y}{a_{3D}} = -\frac{1}{\sqrt{\pi}}\mathcal{F}_1(\epsilon, 0), \quad (4.3)$$

where the right-hand side (RHS) is defined by the definite integral

$$\mathcal{F}_1(\epsilon, 0) = \int_0^\infty dt \left[\frac{\sqrt{\eta} \exp(\epsilon t/2)}{\sqrt{t(1-e^{-\eta t})(1-e^{-t})}} - \frac{1}{t^{3/2}} \right]. \quad (4.4)$$

In the strong-binding limit, the limiting behavior of this integral is

$$\lim_{\epsilon \rightarrow -\infty} -\frac{\mathcal{F}_1(\epsilon, 0)}{\sqrt{\pi}} = \sqrt{\frac{2|E_b|}{\hbar\omega_y}}. \quad (4.5)$$

This leads to the free-space three-dimensional binding energy result, Eq. (3.12), as one expects in this limit. Combining Eqs. (3.15) and (4.1), the threshold condition for a *harmonic* trap can be summarized compactly in one equation as

$$\epsilon + N_x\eta + N_y = 0, \quad (4.6)$$

so that

$$\frac{d_y}{a_{3D}} = -\frac{1}{\sqrt{\pi}}\mathcal{F}_1(-[N_x\eta + N_y], 0). \quad (4.7)$$

Further resonances are anticipated if we consider relative atomic motion. Such an internally excited molecular state is described by a completely different integral equation. For the first excited state of the internal motion, one obtains

$$\frac{d_y}{a_{3D}} = -\frac{1}{\sqrt{\pi}}\mathcal{F}_e(\epsilon_e, 0), \quad (4.8)$$

where the RHS is now defined by the definite integral

$$\begin{aligned} \mathcal{F}_e(\epsilon_e, 0) &= \int_0^\infty dt \left[e^{\epsilon_e t/2} \sqrt{\frac{\eta}{t}} \left(\frac{1}{\sqrt{(1-e^{-\eta t})(1-e^{-t})}} - 1 \right) - \frac{1}{t^{3/2}} \right]. \end{aligned} \quad (4.9)$$

The CIR threshold condition including both internal and c.m. excitations is therefore

$$\epsilon_e + N_x \eta + N_y = 0, \quad (4.10)$$

so that

$$\frac{d_y}{a_{3D}} = -\frac{1}{\sqrt{\pi}} \mathcal{F}_e(-[N_x \eta + N_y], 0). \quad (4.11)$$

Equations (4.6) and (4.10) give threshold conditions in the limit of small anharmonicity, for coupling to either the internal ground or excited state, respectively, with center-of-mass quantum numbers included in the final resonant state.

As such, they give an elegant picture of the possible resonances, including both internal and c.m. excitations. However, if the anharmonic term H_a is not included, the two incoming atoms in a transverse ground state cannot couple to the transverse excited molecular states during the collision. Hence, for harmonic confinement there is only one observable CIR no matter how anisotropic the transverse confinement [19]. This is described by the last equation above, Eq. (4.11), on setting $N_x = N_y = 0$.

In reality, anharmonic terms do occur. These lead both to couplings that allow c.m. excitations and to energy shifts which alter the resonance locations. In the following analysis, we assume that there are only c.m. excitations, and we apply perturbation theory to the bound-state c.m. energies predicted by Eq. (4.6).

B. Anisotropic, anharmonic CIR

If the anharmonic perturbation H_a is now introduced, the c.m. motion is mixed with the relative motion by the anharmonicity of the confining trap. Then the transversely excited c.m. molecular states can couple to the scattering state of the two incoming atoms in the transverse ground state. However, both the atomic and molecular states now have energy levels shifted by anharmonic corrections. This means that the fundamental resonance equation is modified from Eq. (4.6) for the harmonic trap case. It is now

$$\epsilon + N_x \eta + N_y + \epsilon_a(N_x, N_y) = 0, \quad (4.12)$$

where $\epsilon_a(N_x, N_y)$ is the anharmonic correction to the relative energy levels for a c.m. excitation with quantum numbers (N_x, N_y) . This has been treated already in the deeply bound limit in Eq. (3.17). We now treat this in the general case.

From Eq. (3.8), one must include the input anharmonicity in the atomic levels, which for the case of two atoms in an initial atomic transverse ground state is given by Eq. (3.9). Next, we consider the effects of anharmonicity on the bound or molecular energies.

With a quartic anharmonicity which is symmetric around the origin, there are constraints on the types of coupling that can occur to the c.m. motion. In particular, with a symmetric input state having $N_x = N_y = 0$, one must have a symmetric resonance state. This implies that only even c.m. quantum numbers are strongly coupled. There is also a weak coupling to odd c.m. quantum numbers, caused by cubic anharmonic parameters, which we treat in the next section. The lowest of the strong nonlinear resonances occurs when $(N_x, N_y) = (2, 0)$

or $(0, 2)$. Consequently the resonance splits if the transverse confinement is anisotropic.

We give a detailed calculation of the effects of anharmonic confinement on the bound-state energies of these resonances in the Appendix. Using these results, we arrive at the resonance condition for the $N_x = 2$ state,

$$\begin{aligned} \epsilon + 2\eta + \alpha_x \eta \left(\frac{27}{32} - \frac{5\eta}{32\epsilon} + \frac{3\eta^2}{320\epsilon^2} \right) \\ + \alpha_y \left(\frac{-9}{32} - \frac{1}{32\epsilon} + \frac{3}{320\epsilon^2} \right) = 0. \end{aligned} \quad (4.13)$$

In like manner, the resonance condition for the $N_y = 2$ state is

$$\begin{aligned} \epsilon + 2 + \alpha_x \eta \left(\frac{-9}{32} - \frac{\eta}{32\epsilon} + \frac{3\eta^2}{320\epsilon^2} \right) \\ + \alpha_y \left(\frac{27}{32} - \frac{5}{32\epsilon} + \frac{3}{320\epsilon^2} \right) = 0. \end{aligned} \quad (4.14)$$

These results can be compared with those of Eq. (3.17), which were obtained in the previous section dealing with the case of a deeply bound molecular state. On dropping terms scaling with $1/\epsilon$, the two conditions agree in the limit of strong molecular binding, with $\epsilon \rightarrow -\infty$.

For experiments using optical lattices with equal wavelengths in each direction, one finds that

$$\alpha_x \eta = \alpha_y \equiv \alpha. \quad (4.15)$$

Then the resonance conditions can be reduced to a simpler form. For $(N_x, N_y) = (2, 0)$, one obtains

$$\epsilon + 2\eta + \alpha \left(\frac{9}{16} - \frac{5\eta + 1}{32\epsilon} + \frac{3(\eta^2 + 1)}{320\epsilon^2} \right) = 0, \quad (4.16)$$

and for $(N_x, N_y) = (0, 2)$,

$$\epsilon + 2 + \alpha \left(\frac{9}{16} - \frac{\eta + 5}{32\epsilon} + \frac{3(\eta^2 + 1)}{320\epsilon^2} \right) = 0. \quad (4.17)$$

Solving these equations requires the use of a nonlinear-equation-solving numerical algorithm, like the Newton-Raphson method, which we use in Fig. 3 to obtain theoretical results for comparison with experiment.

Now we are ready to understand the dominant effects observed in the recent Innsbruck experiment [23]. The atoms are prepared in a 1D tube geometry using two orthogonal pairs of counterpropagating laser fields to create a trapping environment. In the case of transverse isotropic confinement, due to the small collision energy and large energy interval between the transverse energy levels, only the first excited molecular states $(N_x = 2, N_y = 0)$ and $(N_x = 0, N_y = 2)$ of the c.m. motion which are degenerate can couple to the scattering state of two incoming atoms. In this isotropic situation, the results of ACIR are similar to those of HCIR and also agree well with the experiment, as long as the anharmonicity of the confinement is not too large. Owing to the broad resonances and fitting techniques used, the isotropic experimental data have too little precision to accurately distinguish between ACIRs and CIRs.

By increasing the transverse anisotropy $\eta = \omega_x/\omega_y$, the molecular states $(N_x = 2, N_y = 0)$ and $(N_x = 0, N_y = 2)$ of the c.m. motion are no longer degenerate. A splitting of the

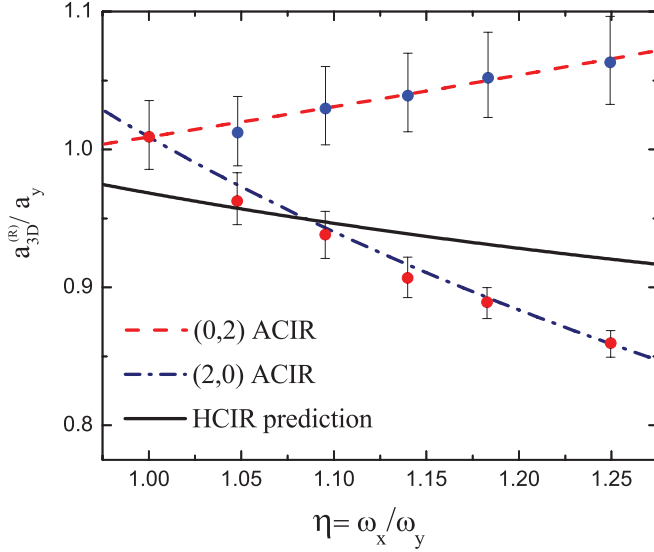


FIG. 3. (Color online) The predictions of ACIRs using first-order anharmonic perturbation theory comparing with the experimental data [23]. The black solid curve is the result of a generalized Olshanii HCIR model [19]. Here the anisotropy η is changed by increasing the frequency ω_x with a fixed $\omega_y = 2\pi \times 13.2(2)$ kHz (or ω_1 in Ref. [23]), which resulted in an anharmonic parameter of $\alpha = -0.133$.

ACIR is expected, which has been observed in the experiment. By contrast, no splitting of the linear HCIR is predicted. Thus, the double resonance observed experimentally is a clear signature of the ACIR. It is also a sign that if there is any internally excited HCIR effect in this experiment, it is relatively suppressed compared to the ACIR effect, which involves c.m. excitations.

The theoretical predictions of the CIRs compared with the experimental results [23] are presented in Fig. 3. As we can see, the predictions of the c.m.-relative coupling theory are consistent with the experimental data.

In these experiments, the resonances were identified as occurring at the point of maximum molecular loss. This leads to an offset between the apparent and true resonance due to finite resonance widths. To compensate for this in the original experimental publication, the data were fitted to the isotropic HCIR prediction by adding a small constant offset to make it equal to the theoretical results at $\eta = 1$. We follow a similar fitting procedure here, for consistency, but we fit the offset to the isotropic ACIR prediction instead. Note that the anharmonic parameter is different from that used in Table I, because Table I gives values representative of a range of experiments, while in each of the figures we use the data from the relevant experiment.

At the point $\eta = 1$, there is transversely *isotropic* confinement, and the ACIR prediction is in accord with the Olshanii CIR, apart from anharmonic corrections. However, as the transverse confinement becomes more and more anisotropic, the internally excited HCIR persists as a single resonance except for a small frequency shift [19]. Both ACIR theory and experiment show a clear splitting of the original resonance with increasing trap asymmetry. There is excellent quantitative agreement in the amount of splitting. In these experiments, there is strong evidence for the c.m. excited ACIRs.

C. Multiple-resonance ACIR at large anisotropy

As the transverse anisotropy η becomes even larger, the energy spacing in the y direction decreases, and more transversely excited molecular states can readily couple to the initial scattering state. Consequently, more additional c.m. resonances can occur. By contrast, there is still only one internal HCIR predicted no matter how large the transverse anisotropy. However, several multiple resonances are observed experimentally at large anisotropy. In order to understand these, we now consider the other transverse states.

As in the previous section, given any coupling parameter (a_{3D}), the unperturbed binding energy ϵ is determined by Eq. (4.3), which as an implicit equation involving the integral $\mathcal{F}_1(\epsilon, 0)$. We then use perturbation theory to calculate the dimensionless anharmonic energy shift ϵ_a . Hence, we obtain the ACIR position of a_{3D} for arbitrary odd and even c.m. quantum numbers from the solutions to the overall resonance equation, Eq. (4.12).

For brevity, we refer to an arbitrary molecular c.m. resonance as simply (N_x, N_y) . The general form of the resulting anharmonic shifts is derived in the Appendix for arbitrary quartic anharmonic parameters. We include both odd- and even-order resonances because, as remarked earlier, there are both cubic and quartic anharmonic couplings, which leads to the possibility of both even and odd ACIRs. However, for simplicity we do not include the relatively small cubic energy shifts.

For comparison to current experiments, we are interested in the case of equal optical trapping wavelengths, which means that $\alpha_x \eta = \alpha_y \equiv \alpha$. From the Appendix, the general form of the resulting anharmonic shifts for resonances corresponding to the (N_x, N_y) c.m. state is as follows:

$$\epsilon_a(N_x, N_y)/\alpha = \frac{3(N_y^2 + N_y + N_x^2 + N_x) - 9}{16} - \frac{2N_y + 1 + \eta(2N_x + 1)}{32\epsilon} + \frac{3(\eta^2 + 1)}{320\epsilon^2}. \quad (4.18)$$

This allows the positions of the ACIR denoted by a_{3D} to be calculated. In the experimental reports of multiple resonances at large anisotropy (Fig. 4 [23]), the loss rates are plotted as a function of magnetic field, rather than a_{3D} . We therefore make use of the relation between the 3D scattering length a_{3D} and B field for the relevant ^{137}Cs Feshbach resonance [31], which is

$$\frac{a_{3D}}{a_{bg}} = \frac{B - 18.1}{B + 11.1} \frac{B - 47.944}{B - 47.78} \frac{B - 53.457}{B - 53.449} \quad (4.19)$$

and

$$\frac{a_{3D}}{a_{bg}} = \frac{1}{1875a_0} \sqrt{\frac{\hbar\eta}{m\omega_x}} \frac{a_{3D}}{a_y} = 0.681\sqrt{\eta} \frac{a_{3D}}{a_y}. \quad (4.20)$$

Hence, the predicted magnetic field at resonance can be calculated. In order to compare our theory to these experiments, the regime of anisotropy η considered is [1.4, 2.3]. We also note that in these experiments the trapping frequency ω_y is

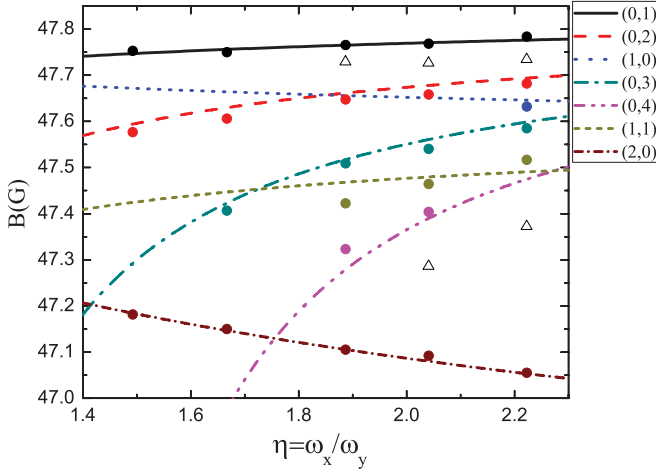


FIG. 4. (Color online) The resonant magnetic field B vs anisotropy η at ACIRs (solid and dotted lines identified alongside the figure) from first-order anharmonic perturbation theory comparing with the Innsbruck experimental data (circles). Data are extracted from multiple resonance scans [23] at absorption edges. Here the anisotropy η is changed by decreasing the frequency ω_y with a fixed $\omega_x = 2\pi \times 16.6(2)$ kHz, which results in an η -dependent anharmonic parameter $\alpha = -0.106\eta$.

varied, so the effective anharmonicity parameter α therefore changes at different anisotropy.

Then main results are summarized in Fig. 4, which compares theory to experiment. The experimental resonance points are obtained from the raw data as the start of the resonance edges, which is appropriate for this type of resonance experiment. No fitting parameters or shifts are employed. Since error bars were not given in the experimental plot, we are unable to estimate these.

Most observed resonances can be easily identified, which are coded in the same color as the corresponding theoretical predictions. There are 25 identified resonances, all of which are in excellent agreement with theoretical calculations. However, there are 5 smaller resonances not identified, which are indicated by the open triangles.

Apart from experimental issues, possible explanations for these unidentified peaks include the following.

Higher-order many-body ACIRs. Combination four-body cluster resonances could occur at intermediate points between the identified two-body resonances. For example, the three unidentified resonances between (0,1) and (0,2) could be caused by the simultaneous excitation of (0,1) and (0,2) in a four-body collision. Similarly, the three resonances we have identified as (1,1) resonances could also be caused by four-body excitation of (0,3) and (0,4) ACIRs.

Anharmonically shifted internal HCIRs. We have not calculated these, as the anharmonic shifts of these resonances are outside the scope of this paper. However, this mechanism provides a possible explanation for the two unidentified resonances between (0,4) and (2,0).

V. ANHARMONIC CIR IN A QUASI-2D SYSTEM

For a quasi-2D system, atoms are tightly confined in the axial direction and can freely move in two transverse

directions. In the following section, we derive the anharmonic CIR properties in this case as well. As we show, these results can be also obtained from results in the previous section by taking one of the confinement frequencies to zero. However, the direct calculation given here is an important check on the consistency of our approach. In the case of an optical lattice, the trapping potential is of the form

$$U^{\text{ext}}(\mathbf{r}) = V_z \cos^2\left(\frac{2\pi z}{\lambda}\right) \approx \frac{1}{2}m\omega^2 z^2 \left(1 + \frac{\alpha z^2}{d^2}\right). \quad (5.1)$$

Here, V_z is the potential well depth with one standing-wave trapping laser at optical wavelength λ . This leads to the trap frequency ω in the z direction. We note that cubic anharmonic terms are also possible due to focusing effects in this case.

As before, we use a scale length of the reduced oscillator length $d = \sqrt{2\hbar/m\omega}$ and define a single-atom oscillator length $a_{\perp} = \sqrt{\hbar/m\omega}$, and a small anharmonic parameter α , so that for an optical lattice

$$\alpha = \frac{-8\pi^2\hbar}{3\lambda^2 m\omega}. \quad (5.2)$$

The Hamiltonian of two atoms in a quasi-2D system is then

$$H = H_1 + H_2 + U(\mathbf{r}_1 - \mathbf{r}_2), \quad (5.3)$$

where

$$H_i = -\frac{\hbar^2}{2m}\nabla_{\mathbf{r}_i}^2 + \frac{1}{2}m\omega^2 z_i^2 \left(1 + \alpha \frac{z_i^2}{d^2}\right) \quad (i = 1, 2). \quad (5.4)$$

As previously, $U(\mathbf{r}_1 - \mathbf{r}_2)$ is the interatomic interaction, and we set

$$\begin{aligned} \mathbf{R} &= \frac{1}{2}(\mathbf{r}_1 + \mathbf{r}_2), \\ \mathbf{r} &= \mathbf{r}_1 - \mathbf{r}_2. \end{aligned} \quad (5.5)$$

Then Eq. (5.3) becomes

$$H = H_h + H_a, \quad (5.6)$$

where

$$\begin{aligned} H_h &= \left(-\frac{\hbar^2}{2M}\nabla_{\mathbf{R}}^2 + \frac{1}{2}M\omega^2 Z^2\right) \\ &\quad + \left[-\frac{\hbar^2}{2\mu}\nabla_{\mathbf{r}}^2 + \frac{1}{2}\mu\omega^2 z^2 + V(\mathbf{r})\right] \\ &= H_h^{\text{c.m.}} + H_h^{\text{rel}} \end{aligned} \quad (5.7)$$

$$H_a = \alpha \frac{m\omega^2}{2d^2} \left(2Z^4 + 3Z^2 z^2 + \frac{1}{8}z^4\right). \quad (5.8)$$

Here $\mathbf{r} = (x, y, z)$, $\mathbf{R} = (X, Y, Z)$, and $M = 2m$, $\mu = m/2$.

Owing to the small anharmonic parameter α , the anharmonic term H_a can be treated as a perturbation to H_h . First, consider the case without the small perturbation H_a . An anharmonic confinement-induced resonance is expected when the energy of the virtual molecule is degenerate with the energy of two incoming atoms from the axial ground state,

$$E_M^{(0)} = E_{\text{c.m.}} + E_b = E_{\text{scatt}}, \quad (5.9)$$

where $E_{c.m.} = (N + \frac{1}{2})\hbar\omega$, $E_{scatt} = \hbar\omega$, the binding energy E_b is determined by

$$\frac{d}{a_{3D}} = -\frac{1}{\sqrt{\pi}}\mathcal{F}_2(\epsilon, 0), \quad (5.10)$$

and the integral expression required here is given by

$$\mathcal{F}_2(\epsilon, 0) = \int_0^\infty dt \left[\frac{\exp(\frac{1}{2}\epsilon t)}{t\sqrt{1-e^{-t}}} - \frac{1}{t^{3/2}} \right]. \quad (5.11)$$

We define $E_b = (\epsilon + 1/2)\hbar\omega$, $d = \sqrt{\hbar/\mu\omega}$. The lowest resonance occurs as $N = 2$; however, this is not coupled to the incoming states unless there is an anharmonic term in the potential.

If the anharmonic term H_a is included, we need to consider how the energy of the input atomic states and virtual molecule E_M is affected by this perturbation.

A. The anharmonic energy $E_M^{(1)}$

Including the first-order modification $E_M^{(1)}$, we arrive at the following integral equation for ϵ :

$$(N + \frac{1}{2})\hbar\omega + (\epsilon + \frac{1}{2})\hbar\omega + E_M^{(1)}(\epsilon) = \hbar\omega + \frac{3}{8}\alpha\hbar\omega. \quad (5.12)$$

By solving this equation, the binding energy $\epsilon^{(R)}$ at the resonance is obtained. Then substituting $\epsilon^{(R)}$ into Eq. (5.10), we obtain the 3D scattering length $a_{3D}^{(R)}$ at the resonance. Following the general procedure outlined in the Appendix, we find that a resonance occurs at

$$N + \epsilon + \frac{\alpha}{32} \left[6N(N+1) - 9 - \frac{(2N+1)}{\epsilon} + \frac{3}{10\epsilon^2} \right] = 0. \quad (5.13)$$

Hence, we obtain the equation that ϵ should satisfy for states with $N = 2$,

$$\epsilon + 2 + \alpha \left(\frac{27}{32} - \frac{5}{32\epsilon} + \frac{3}{320\epsilon^2} \right) = 0. \quad (5.14)$$

This result is identical to Eq. (4.14) in the limit of $\eta \rightarrow 0$, as one might expect, since the quasi-1D trap becomes two-dimensional in this limit. However, it is instructive that one cannot regain this limit directly from Eq. (4.17), which holds for optical lattices with equal wavelengths. The reason is very simple: in an optical lattice at low transverse confinement frequency, the transverse wave function becomes more and more deconfined. This increases the relative anharmonicity, as given in Eq. (3.4), so that $\alpha \sim 1/\omega$. Therefore, our anharmonic perturbation theory would break down for a weakly confined 1D system described by Eq. (4.17). Optical lattices that are only weakly confining require a full Bloch wave-function theory, typically requiring detailed numerical diagonalization [32].

From Eq. (5.14), we can calculate the relative binding energy ϵ for the states of $N = 2$ in the two-dimensional limit. Then, substituting into Eq. (5.10), the corresponding resonance scattering length $a_{3D}^{(R)}$ is obtained. Here, in order to calculate ϵ numerically, we use the Newton-Raphson method as before, together with a numerical calculation of $\mathcal{F}_2(\epsilon, 0)$. The position

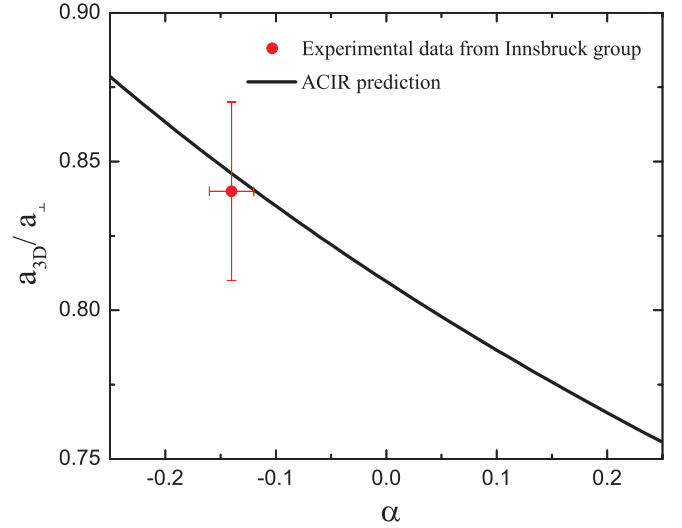


FIG. 5. (Color online) Predicted resonance positions of 2D CIRs as a function of the dimensionless anharmonic parameter α . The experimental data point is an average from experiments [23], plotted at the average anharmonicity value.

of the ACIR denoted by the 3D scattering length as a function of the anharmonic parameter αd^2 is presented in Fig. 5, and we can see that the 2D ACIR is predicted at the regime of $a_{3D} > 0$. This is in contrast to the internal HCIR, which occurs for the attractive regime with $a_{3D} < 0$.

Now we can compare these predictions with 2D resonances observed in the recent Innsbruck experiment [23]. When one of the lattice lasers is turned off, the system approaches a 2D geometry. All resonances disappear except one at $a_{3D} > 0$. Given the average anharmonicity in this experiment of $\alpha = -0.121$, we expect as shown in Fig. 5 to find a resonance at

$$a_{3D} = 0.85a_{\perp}. \quad (5.15)$$

The observed resonances occur at a constant ratio between a_{3D} and a_{\perp} , such that

$$\frac{a_{3D}}{a_{\perp}} a_{3D} = 0.84(3). \quad (5.16)$$

This is consistent with the prediction of 2D ACIR. The anharmonicity α in the experiments was varied through a small range as the trapping frequency varied, and we have calculated the ratio at the average anharmonicity.

Finally, we plot the predicted variation of $a_{3D}^{(R)}$ with transverse confinement parameter a_{\perp} , at a fixed value of $\omega\alpha$ corresponding to the Innsbruck experiments, in Fig. 6. These data are also in excellent quantitative agreement with ACIR predicted resonance positions.

In anharmonic trap experiments, we would generically expect both the ACIR at $a_{3D} > 0$ and the internal HCIR at $a_{3D} < 0$ to be observed. The Innsbruck experiments [23] show clear evidence for the ACIR but not the internal HCIR. The Cambridge experiments [24] have shown evidence for HCIRs, although the magnetic field scans were not large enough to observe any ACIRs. The question of which is observed depends on the size of the anharmonic parameter, the dynamics of the experiment, and the method of detection of the

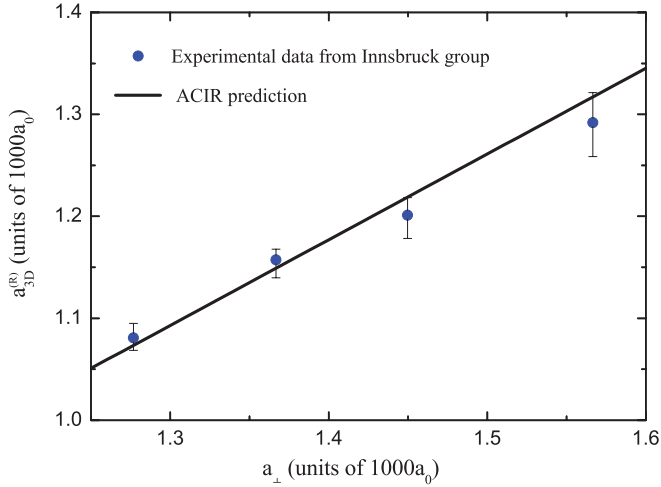


FIG. 6. (Color online) Predicted resonance positions of 2D ACIRs as a function of the transverse confinement parameter, a_{\perp} . The experimental data points are taken from [23], where circles indicate resonances identified by absorption edges.

resonance. It appears likely that the molecular loss technique is particularly sensitive to c.m. resonances.

VI. CONCLUSION

We have extended the theory of the harmonic confinement-induced resonance to include the effects of anharmonic confinement, or ACIR, since previous harmonic theories cannot explain the phenomena observed in recent experiments. In the presence of anharmonic perturbation of the confinement trap, the c.m. motion of two atoms couples to the relative motion, and additional resonances appear. We have calculated the energy of the resulting resonances up to first order in perturbation theory. The results agree well with experiments, with both even- and odd-order multiple resonances being found. These differences are not just small perturbations on previous HCIR predictions, and they show large qualitative differences from the predictions for harmonic traps.

ACIRs due to c.m. excitations are always present in Feshbach systems with any form of transverse confinement. The important issue is that for harmonic traps the Kohn theorem prevents these resonances from being coupled to incoming atoms in the two-body sector of the c.m. ground state. However, experimental optical traps do have relatively large anharmonic parameters, which allows the resonances due to c.m. motion to be coupled to incoming scattering states. We find excellent quantitative agreement between ACIR predictions and recent experimental observations of confinement resonances, in both one- and two-dimensional traps.

ACKNOWLEDGMENTS

This work was supported by the ARC Discovery Projects No. DP0984637, No. DP0880404, and No. DP0984522, and NFRPC Grant No. 2011CB921502. One of us, P.D.D., wishes to thank the Aspen Center for Physics for their generous hospitality. We also wish to acknowledge useful discussions

and communications with C. Vale, H.-C. Nagerl, R. Grimm, M. Kohl, S. Sala, P.-I. Schneider, and A. Saenz.

APPENDIX: ANHARMONIC PERTURBATION THEORY

We consider how the relative anharmonic energy of the virtual molecule ϵ_a , Eq. (4.12), is calculated from the anharmonic perturbation H_a , including the effects of anharmonicity on both relative and c.m. motion. For space reasons, we do not give all the overlap integrals, as the calculations are similar in all cases. Instead, we focus on the most important cases.

First, note that the dimensionless change in the relative anharmonic perturbation energy is

$$\epsilon_a = \frac{1}{\hbar\omega_y} [E_M^{(1)} - 2E_A^{(1)}], \quad (\text{A1})$$

where $E_A^{(1)}$ is the perturbed atomic anharmonic energy given in Eq. (3.8), and $E_M^{(1)}$ is the first-order perturbation theory correction to the energy of the virtual molecule:

$$E_M^{(1)} = \langle \Psi_{N_x N_y} \psi_b | H_a | \psi_b \Psi_{N_x N_y} \rangle. \quad (\text{A2})$$

Here, $|\Psi_{N_x N_y} \psi_b\rangle = |\Psi_{N_x N_y}\rangle |\psi_b\rangle$ is the eigenstate of H_h . This is treated as the zero-order wave function and includes both relative and c.m. motion. Next, we introduce $|\Psi_{N_x N_y}\rangle$ as the unperturbed wave function of the c.m. Hamiltonian, so that

$$|\Psi_{N_x N_y}\rangle = |\phi_{N_x}\rangle |\phi_{N_y}\rangle \quad (\text{A3})$$

with the standard two-dimensional harmonic oscillator solution of

$$|\phi_{N_{x,y}}\rangle = \frac{\exp(-2\xi_{x,y}^2) H_{N_{x,y}}(2\xi_{x,y})}{\sqrt{\pi^{1/2} d_{x,y} 2^{N_{x,y}-1} N_{x,y}!}}, \quad (\text{A4})$$

where $\xi_i = (X/d_x, Y/d_y)$. We now turn to the task of evaluating $E_M^{(1)}$, the anharmonic correction to the total molecular energy at a given unperturbed dimensionless energy ϵ .

1. The relative wave function $|\psi_b\rangle$

The specific form of $|\psi_b\rangle$ can be obtained by directly solving the eigenproblem of H_h^{rel} ,

$$\left[-\frac{\hbar^2}{2\mu} \nabla_{\mathbf{r}}^2 + \frac{1}{2} \mu \omega_x^2 x^2 + \frac{1}{2} \mu \omega_y^2 y^2 + V(\mathbf{r}) \right] |\psi\rangle = E |\psi\rangle. \quad (\text{A5})$$

The wave function $|\psi\rangle$ can be written as

$$\begin{aligned} |\psi\rangle &= \psi_0(\mathbf{r}) - \int_0^\infty d\mathbf{r}' G_E(\mathbf{r}, \mathbf{r}') V(\mathbf{r}') \psi(\mathbf{r}') \\ &= \psi_0(\mathbf{r}) - \mathcal{R} \cdot \frac{2\pi\hbar^2 a_{3D}}{\mu} G_E(\mathbf{r}, 0), \end{aligned} \quad (\text{A6})$$

where $\psi_0(\mathbf{r})$ is the regular solution of Eq. (A5) and

$$\mathcal{R} = \left[\frac{\partial}{\partial r} r \psi(\mathbf{r}) \right]_{r=0}. \quad (\text{A7})$$

Here, we have used the pseudopotential approximation. For a bound state, the solution of Eq. (A5) $|\psi\rangle$ should vanish as $r \rightarrow \infty$; hence, $\psi_0(\mathbf{r}) = 0$. Then the constant \mathcal{R} is only a

normalization coefficient. The Green's function $G_E(\mathbf{r}, \mathbf{r}')$ is the solution of the following equation:

$$\left[-\frac{\hbar^2}{2\mu} \nabla_{\mathbf{r}}^2 + \frac{1}{2} \mu \omega_x^2 x^2 + \frac{1}{2} \mu \omega_y^2 y^2 - E \right] G_E(\mathbf{r}, \mathbf{r}') = \delta(\mathbf{r} - \mathbf{r}'). \quad (\text{A8})$$

The form of the Green's function $G_E(\mathbf{r}, 0)$ for a bound state can be easily calculated,

$$G_{\epsilon < 0}(\mathbf{r}, 0) = \frac{\sqrt{\eta} I_1(\mathbf{r})}{2\pi^{3/2} d^3 \hbar \omega_y} \exp\left(-\frac{\eta x^2 + y^2}{2d^2}\right), \quad (\text{A9})$$

where we introduce the integral representation,

$$I_1(\mathbf{r}) = \int_0^\infty dt \frac{\exp\left(\frac{\epsilon}{2}t - \frac{1}{t} \frac{z^2}{d^2} - \frac{e^{-\eta t}}{1-e^{-\eta t}} \frac{\eta x^2}{d^2} - \frac{e^{-t}}{1-e^{-t}} \frac{y^2}{d^2}\right)}{\sqrt{t(1-e^{-\eta t})(1-e^{-t})}}. \quad (\text{A10})$$

Recalling that $\eta = \omega_x/\omega_y$, and $E = (\epsilon + \eta/2 + 1/2)\hbar\omega_y$, the bound-state wave function is

$$|\psi_b\rangle = \mathcal{N} \exp\left(-\frac{\eta x^2 + y^2}{2d^2}\right) I(\mathbf{r}), \quad (\text{A11})$$

where \mathcal{N} is the normalization coefficient.

2. 1D c.m. overlap terms

We can now calculate the overlap integrals which give the anharmonic contributions to the quasi-1D and quasi-2D ACIRs. In order to calculate the first-order modification $E_M^{(1)}$, we focus on the (N_x, N_y) c.m. state. The relevant terms are $\langle \Psi_{N_x N_y} | X^4 | \Psi_{N_x N_y} \rangle$, $\langle \Psi_{N_x N_y} | Y^4 | \Psi_{N_x N_y} \rangle$, $\langle \Psi_{N_x N_y} | X^2 | \Psi_{N_x N_y} \rangle$, and $\langle \Psi_{N_x N_y} | Y^2 | \Psi_{N_x N_y} \rangle$.

We define $D_{x,y} = \sqrt{\hbar/2m\omega_{x,y}} = d_{x,y}/2$ as the transverse confinement parameter of an atom pair in the following calculation. Hence:

$$\begin{aligned} \langle \psi_{N_x N_y} | X^4 | \psi_{N_x N_y} \rangle &= \frac{1}{\sqrt{\pi} D_x 2^{N_x} N_x!} \int_{-\infty}^{\infty} X^4 \exp\left(-\frac{X^2}{D_x^2}\right) \left[H_{N_x}\left(\frac{X}{D_x}\right) \right]^2 dX \\ &= \frac{1}{\sqrt{\pi} D_x 2^{N_x} N_x!} D_x^5 \sqrt{\pi} 2^{N_x} N_x! \left[\left(N_x + \frac{1}{2}\right) \left(N_x + \frac{3}{2}\right) + \frac{1}{2} N_x (N_x - 1) \right] \\ &= \left[\left(N_x + \frac{1}{2}\right) \left(N_x + \frac{3}{2}\right) + \frac{1}{2} N_x (N_x - 1) \right] D_x^4, \end{aligned} \quad (\text{A12})$$

$$\begin{aligned} \langle \psi_{N_x N_y} | X^2 | \psi_{N_x N_y} \rangle &= \frac{1}{\sqrt{\pi} D_x 2^{N_x} N_x!} \int_{-\infty}^{\infty} X^2 \exp\left(-\frac{X^2}{D_x^2}\right) \left[H_{N_x}\left(\frac{X}{D_x}\right) \right]^2 dX \\ &= \frac{1}{\sqrt{\pi} D_x 2^{N_x} N_x!} D_x^3 \sqrt{\pi} 2^{N_x} N_x! \left(N_x + \frac{1}{2}\right) = \left(N_x + \frac{1}{2}\right) D_x^2. \end{aligned} \quad (\text{A13})$$

By using the exchange symmetry of x and y , we can easily obtain

$$\langle \psi_{N_x N_y} | Y^4 | \psi_{N_x N_y} \rangle = \left[\left(N_y + \frac{1}{2}\right) \left(N_y + \frac{3}{2}\right) + \frac{1}{2} N_y (N_y - 1) \right] D_y^4, \quad (\text{A14})$$

$$\langle \psi_{N_x N_y} | Y^2 | \psi_{N_x N_y} \rangle = \left(N_y + \frac{1}{2}\right) D_y^2. \quad (\text{A15})$$

Here, we have used the formulas

$$\int_{-\infty}^{\infty} dt t^2 e^{-t^2} H_n^2(t) = \sqrt{\pi} 2^n n! \left(n + \frac{1}{2}\right), \quad (\text{A16})$$

$$\int_{-\infty}^{\infty} dt t^4 e^{-t^2} H_n^2(t) = \sqrt{\pi} 2^n n! \left[\left(n + \frac{1}{2}\right) \left(n + \frac{3}{2}\right) + \frac{1}{2} n(n-1) \right]. \quad (\text{A17})$$

3. 1D internal motion overlap terms

The relevant terms are now $\langle \psi_b | x^4 | \psi_b \rangle$, $\langle \psi_b | y^4 | \psi_b \rangle$, $\langle \psi_b | x^2 | \psi_b \rangle$, and $\langle \psi_b | y^2 | \psi_b \rangle$. For the bound state of the relative motion $|\psi_b\rangle$, the main contribution of the integrals, e.g., $\langle \psi_b | x^4 | \psi_b \rangle$, etc., comes from the regime around the origin. We note that the energy parameter ϵ is negative. The form of $|\psi_b\rangle$ near the origin $r = 0$ can be easily obtained from Eq. (A11),

$$|\psi_b\rangle \approx \left(\frac{-\epsilon}{2}\right)^{1/4} \frac{1}{\sqrt{\pi} d_y} \frac{\exp(-\sqrt{-2\epsilon}r/d_y)}{r}, \quad (\text{A18})$$

which has been normalized. Then,

$$\langle \psi_b | x^2 | \psi_b \rangle = \frac{1}{\pi d_y} \sqrt{\frac{-\epsilon}{2}} \int_0^{2\pi} \int_0^\pi \int_0^\infty r^2 \sin^3 \theta \cos^2 \phi \exp\left(-\frac{2\sqrt{-2\epsilon}r}{d_y}\right) dr d\theta d\phi = -\frac{d_y^2}{12\epsilon}, \quad (\text{A19})$$

$$\langle \psi_b | x^4 | \psi_b \rangle = \frac{1}{\pi d_y} \sqrt{\frac{-\epsilon}{2}} \int_0^{2\pi} \int_0^\pi \int_0^\infty r^4 \sin^4 \theta \cos^4 \phi \frac{\exp(-2\sqrt{-2\epsilon}r/d_y)}{r^2} r^2 \sin \theta dr d\theta d\phi = \frac{3d_y^4}{40\epsilon^2}, \quad (\text{A20})$$

$$\langle \psi_b | y^2 | \psi_b \rangle = \frac{1}{\pi d_y} \sqrt{\frac{-\epsilon}{2}} \int_0^{2\pi} \int_0^\pi \int_0^\infty r^2 \sin^2 \theta \sin^2 \phi \frac{\exp(-2\sqrt{-2\epsilon r/d_y})}{r^2} r^2 \sin \theta dr d\theta d\phi = -\frac{d_y^2}{12\epsilon}, \quad (\text{A21})$$

$$\langle \psi_b | y^4 | \psi_b \rangle = \frac{1}{\pi d_y} \sqrt{\frac{-\epsilon}{2}} \int_0^{2\pi} \int_0^\pi \int_0^\infty r^4 \sin^4 \theta \sin^4 \phi \frac{\exp(-2\sqrt{-2\epsilon r/d_y})}{r^2} r^2 \sin \theta dr d\theta d\phi = \frac{3d_y^4}{40\epsilon^2}. \quad (\text{A22})$$

4. The first-order modification of the energy $E_M^{(1)}$

Using the overlap integral results given above, we find that

$$\langle \psi_{N_x N_y} \psi_b | H_a^x | \psi_{N_x N_y} \psi_b \rangle = \frac{\alpha_x \hbar \omega_x}{32} \left[6N_x(N_x + 1) + 3 - \frac{\eta(2N_x + 1)}{\epsilon} + \frac{3\eta^2}{10\epsilon^2} \right], \quad (\text{A23})$$

$$\langle \psi_{N_x N_y} \psi_b | H_a^y | \psi_{N_x N_y} \psi_b \rangle = \frac{\alpha_y \hbar \omega_y}{32} \left[6N_y(N_y + 1) + 3 - \frac{(2N_y + 1)}{\epsilon} + \frac{3}{10\epsilon^2} \right]. \quad (\text{A24})$$

Combining this with the atomic energy correction gives the overall result for an equal-wavelength 1D optical lattice, in which $\alpha_x \omega_x = \alpha_y \omega_y$:

$$\epsilon_a^{(1D)} = \frac{\alpha}{32} \left[6(N_y^2 + N_y + N_x^2 + N_x) - 18 - \frac{\eta(2N_x + 1) + (2N_y + 1)}{\epsilon} + \frac{3(\eta^2 + 1)}{10\epsilon^2} \right]. \quad (\text{A25})$$

Following similar procedures, from Eq. (A24), the anharmonic correction in the corresponding 2D case leads to

$$\epsilon_a^{(2D)} = \frac{\alpha}{32} \left[6N(N + 1) - 9 - \frac{(2N + 1)}{\epsilon} + \frac{3}{10\epsilon^2} \right]. \quad (\text{A26})$$

-
- [1] M. D. Girardeau, *J. Math. Phys.* **1**, 516 (1960); *Phys. Rev.* **139**, B500 (1965).
- [2] E. H. Lieb and W. Liniger, *Phys. Rev.* **130**, 1605 (1963); E. H. Lieb, *ibid.* **130**, 1616 (1963).
- [3] C. N. Yang and C. P. Yang, *J. Math. Phys.* **10**, 1115 (1969).
- [4] D. M. Gangardt and G. V. Shlyapnikov, *Phys. Rev. Lett.* **90**, 010401 (2003).
- [5] K. V. Kheruntsyan, D. M. Gangardt, P. D. Drummond, and G. V. Shlyapnikov, *Phys. Rev. Lett.* **91**, 040403 (2003); *Phys. Rev. A* **71**, 053615 (2005).
- [6] B. Laburthe Tolra, K. M. O'Hara, J. H. Huckans, W. D. Phillips, S. L. Rolston, and J. V. Porto, *Phys. Rev. Lett.* **92**, 190401 (2004).
- [7] T. Kinoshita, T. R. Wenger, and D. S. Weiss, *Science* **305**, 1125 (2004).
- [8] E. Haller, M. Gustavsson, M. J. Mark, J. G. Danzl, R. Hart, G. Pupillo, and H. C. Nagerl, *Science* **325**, 1224 (2009).
- [9] V. L. Berezinskii, *Zh. Eksp. Teor. Fiz.* **59**, 907 (1970) [*Sov. Phys. JETP* **32**, 493 (1971)].
- [10] J. M. Kosterlitz and D. J. Thouless, *J. Phys. C* **6**, 1181 (1973).
- [11] Z. Hadzibabic, P. Kruger, M. Cheneau, B. Battelier, and J. Dalibard, *Nature (London)* **441**, 1118 (2006).
- [12] H. Feshbach, *Ann. Phys. (NY)* **5**, 357 (1958).
- [13] T. Kohler, K. Goral, and P. S. Julienne, *Rev. Mod. Phys.* **78**, 1311 (2006).
- [14] I. Bloch, J. Dalibard, and W. Zwerger, *Rev. Mod. Phys.* **80**, 885 (2008).
- [15] M. Olshanii, *Phys. Rev. Lett.* **81**, 938 (1998).
- [16] T. Bergeman, M. G. Moore, and M. Olshanii, *Phys. Rev. Lett.* **91**, 163201 (2003).
- [17] Y. Nishida and S. Tan, *Phys. Rev. Lett.* **101**, 170401 (2008); *Phys. Rev. A* **82**, 062713 (2010).
- [18] G. Lamporesi, J. Catani, G. Barontini, Y. Nishida, M. Inguscio, and F. Minardi, *Phys. Rev. Lett.* **104**, 153202 (2010).
- [19] S.-G. Peng, S. S. Bohloul, X.-J. Liu, H. Hu, and P. D. Drummond, *Phys. Rev. A* **82**, 063633 (2010).
- [20] D. S. Petrov, M. Holzmann, and G. V. Shlyapnikov, *Phys. Rev. Lett.* **84**, 2551 (2000).
- [21] D. S. Petrov and G. V. Shlyapnikov, *Phys. Rev. A* **64**, 012706 (2001).
- [22] P. Naidon, E. Tiesinga, W. F. Mitchell, and P. S. Julienne, *New J. Phys.* **9**, 19 (2007).
- [23] E. Haller, M. J. Mark, R. Hart, J. G. Danzl, L. Reichsollner, V. Melezhik, P. Schmelcher, and H.-C. Nagerl, *Phys. Rev. Lett.* **104**, 153203 (2010). Note that in comparisons with this paper, we use the notation $\omega_x = \omega_2$, $\omega_y = \omega_1$.
- [24] B. Fröhlich, M. Feld, E. Vogt, M. Koschorreck, W. Zwerger, and M. Kohl, *Phys. Rev. Lett.* **106**, 105301 (2011).
- [25] C. Vale (private communication).
- [26] W. Kohn, *Phys. Rev.* **123**, 1242 (1961); J. F. Dobson, *Phys. Rev. Lett.* **73**, 2244 (1994).
- [27] V. Peano, M. Thorwart, C. Mora, and R. Egger, *New J. Phys.* **7**, 192 (2005).
- [28] J. P. Kestner and L. M. Duan, *New J. Phys.* **12**, 11 (2010).
- [29] S. Sala, P.-I. Schneider, and A. Saenz, e-print [arXiv:1104.1561](https://arxiv.org/abs/1104.1561).
- [30] P. D. Drummond, K. V. Kheruntsyan, and H. He, *J. Opt. B* **1**, 387 (1999); K. V. Kheruntsyan and P. D. Drummond, *Phys. Rev. A* **61**, 063816 (2000); P. D. Drummond and K. V. Kheruntsyan, *ibid.* **70**, 033609 (2004).
- [31] A. D. Lange, K. Pilch, A. Prantner, F. Ferlaino, B. Engeser, H. C. Nagerl, R. Grimm, and C. Chin, *Phys. Rev. A* **79**, 013622 (2009).
- [32] H. P. Büchler, *Phys. Rev. Lett.* **104**, 090402 (2010).